Atlantic Ocean Heat Transport Enabled by Indo#Pacific Heat Uptake and Mixing

Geophysical Research Letters

RESEARCH LETTER
10.1029/2019GL085160

Atlantic Ocean Heat Transport Enabled by Indo-Pacific Heat Uptake and Mixing

Ryan M. Holmes[1,2], Jan D. Zika[2], Raffaele Ferrari[3], Andrew F. Thompson[4], Emily R. Newsom[5], and Matthew H. England[1]

[1]Climate Change Research Centre and the ARC Centre of Excellence for Climate Extremes, University of New South Wales, Sydney, New South Wales, Australia, [2]School of Mathematics and Statistics, University of New South Wales, Sydney, New South Wales, Australia, [3]Department of Earth, Atmospheric and Planetary Sciences, Massachusetts Institute of Technology, Cambridge, MA, USA, [4]Environmental Science and Engineering, California Institute of Technology, Pasadena, CA, USA, [5]Department of Physics, University of Oxford, Oxford, UK

Key Points:
- Heat budget analysis reveals links between meridional and diathermal ocean heat transports
- Large fraction of Atlantic northward heat transport is sourced from eastern tropical Pacific heat uptake
- Turbulent mixing transfers heat from warm shallow Indo-Pacific circulation to cold deep-reaching Atlantic circulation

Supporting Information:
- Supporting Information S1

Correspondence to:
R. M. Holmes
ryan.holmes@unsw.edu.au

Citation:
Holmes, R. M., Zika, J. D., Ferrari, R., Thompson, A. F., Newsom, E. R., & England, M. H. (2019). Atlantic Ocean Heat Transport Enabled by Indo-Pacific Heat Uptake and Mixing. *Geophysical Research Letters*, *46*, 13,939–13,949. https://doi.org/10.1029/2019GL085160

Received 27 AUG 2019
Accepted 24 OCT 2019
Accepted article online 3 NOV 2019
Published online 11 DEC 2019

Abstract The ocean transports vast amounts of heat around the planet, helping to regulate regional climate. One important component of this heat transport is the movement of warm water from equatorial regions toward the poles, with colder water flowing in return. Here, we introduce a framework relating meridional heat transport to the diabatic processes of surface forcing and turbulent mixing that move heat across temperature classes. Applied to a (1/4)° global ocean model the framework highlights the role of the tropical Indo-Pacific in the global ocean heat transport. A large fraction of the northward heat transport in the Atlantic is ultimately sourced from heat uptake in the eastern tropical Pacific. Turbulent mixing moves heat from the warm, shallow Indo-Pacific circulation to the cold deeper-reaching Atlantic circulation. Our results underscore a renewed focus on the tropical oceans and their role in global circulation pathways.

1. Introduction

The ocean plays a critical role in the climate system by moving heat between climate zones and sequestering it in the subsurface (Gregory, 2000; Trenberth & Caron, 2001; Trenberth et al., 2019). How this heat transport responds to external forcing due to interannual and decadal natural variability and forced climate change remains a first-order question in climate science.

Studies of ocean heat transport have traditionally focused on the ocean's general circulation (i.e., the circulation of seawater), and how it carries heat with it. The drivers of this circulation still remain under discussion, with debate centering around the proportion of water mass transformation between light and dense waters occurring in the high-latitude North Atlantic and the Southern Ocean and through diapycnal upwelling at lower latitudes (Cessi, 2019; Ferrari & Wunsch, 2009; Ferrari et al., 2017; Gnanadesikan, 1999; Talley, 2013; Lee et al., 2018; Marshall & Speer, 2012; Thompson et al., 2016; Toggweiler et al., 2019; Newsom & Thompson, 2018). Some studies emphasize the importance of an interbasin circulation involving significant exchange of water of differing densities between the Atlantic and Indo-Pacific basins (Ferrari et al., 2017; Thompson et al., 2016) through the Southern Hemisphere supergyre (Gordon, 1986; Gordon et al., 1992; Rintoul, 1991; Speich et al., 2007). In particular, Newsom and Thompson (2018) highlighted the importance of asymmetries in the net buoyancy forcing between the Atlantic and Indo-Pacific, emphasizing the often overlooked role of water mass transformation in the tropical Indo-Pacific for the global residual circulation. However, as emphasized by Forget and Ferreira (2019), connecting ocean heat transport only with the circulation of seawater can be problematic as much of the heat content within a given water parcel remains inaccessible for ocean-atmosphere exchange and simply moves around closed circulation loops, such as the horizontal gyres, unchanged.

The ocean is warmed by air-sea heat fluxes at low latitudes and warm sea surface temperatures and cooled in the mid and high latitudes at colder temperatures (e.g. Speer & Tziperman, 1992; Large & Yeager, 2009; Valdivieso et al., 2017). Therefore, in order to maintain a steady state, heat must be moved not only from low to high latitudes (the ocean's *meridional* heat transport) but also from warm to cold temperatures (the ocean's *diathermal* heat transport). This net downgradient warm-to-cold heat transfer can only be achieved by diffusive mixing processes (e.g. Hieronymus et al., 2014; Niiler & Stevenson, 1982), which act to destroy

the temperature differentials created by air-sea heat fluxes. Holmes et al. (2019a, hereafter HZE19) showed in a global ocean sea ice model that this downgradient diathermal heat transport peaks near 22 °C with a magnitude similar to the peak meridional heat transport. This realization highlights the dependence of the ocean's meridional heat transport on diabatic processes (here we define a diabatic process as any process that changes the temperature of a fluid parcel, including the along-isopycnal diffusive transport of heat resulting from eddy stirring), both surface forcing and turbulent mixing, that influence the temperature of waters that are exchanged across latitude lines by the circulation. However, no comprehensive description of oceanic heat transport pathways that includes diathermal transports yet exists.

A number of studies have attempted to attribute the ocean's meridional heat transport to different aspects of the ocean circulation by introducing various forms of *heat functions* (e.g. Boccaletti et al., 2005; Czaja & Marshall, 2006; Ferrari & Ferreira, 2011; Greatbatch & Zhai, 2007; Saenko et al., 2018; Vallis & Farneti, 2009; Yang et al., 2015; Zika et al., 2013; Zika et al., 2015). Such heat functions quantitatively isolate net ocean heat transports from the passive circulation of heat around closed circulation cells (also see Talley, 2003 for an alternative approach based on water-masses). Ferrari and Ferreira (2011) used a heat function to demonstrate that the ocean's meridional heat transport is controlled largely by winds and mixing within the thermocline and is less sensitive to high-latitude convection or abyssal mixing, which form the traditional focus of studies of the ocean's overturning. While the deep-reaching Atlantic Meridional Overturning Circulation (AMOC) does carry large amounts of heat northward, it remains unclear how and where this heat is supplied, and how the deep-reaching circulation is connected to the shallow wind-driven cells that otherwise dominate the heat transport.

The heat function of Ferrari and Ferreira (2011) provides an intuitive framework in which to evaluate the contribution of different aspects of ocean circulation to the ocean's meridional heat transport. By constructing a complete budget for the heat function in the latitude-temperature plane (section 2), we will show that a similar framework can be used to evaluate the role of different diabatic processes. We apply this budget framework to a comprehensive (1/4)° global ocean sea ice model to evaluate the contribution of diabatic processes occurring in different ocean basins to the ocean's meridional heat transport (sections 3 and 4). We find that, while much of the ocean's northward heat transport occurs in the Atlantic ocean, Indo-Pacific diabatic processes play a critical role by connecting the shallow and deep circulations and providing heat to the AMOC to be carried northward (section 5). Our results are summarized in section 6.

2. A Framework for Studying Ocean Heat transport

In this section we describe an extension of the global diathermal heat transport framework discussed by HZE19 that can be used to study the flow of heat in the temperature-latitude plane.

2.1. Internal Heat Content

We consider the heat budget of the volume of fluid colder than a given temperature Θ and bounded to the north by a latitude ϕ (Figure 1).

The volume (our study will be performed in the context of incompressible Boussinesq model simulations; if the fluid were instead compressible then it would be more appropriate to consider the mass rather than volume (Hochet & Tailleux, 2019; Holmes et al., 2019b)) of this region is

$$\mathcal{V}(\phi,\Theta,t)=\int\int\int_{\Theta'(x',\phi',z',t)<\Theta} H(\phi-\phi')dV', \tag{1}$$

where H is the Heaviside step function and the integral is performed following the temporally and spatially varying temperature field Θ'. The heat content of this volume $\mathcal{H}$ can be represented in terms of an integral in temperature coordinates,

$$\mathcal{H}(\phi,\Theta,t)=\int_{-\infty}^{\Theta}\rho_0 C_p\Theta'\frac{\partial\mathcal{V}}{\partial\Theta'}d\Theta', \tag{2}$$

where ρ_0 is a constant reference density, C_p is a constant "specific heat capacity" (note that the simulations we consider use potential temperature with a constant for C_p and thus make the assumption that potential temperature is conserved within the ocean, which is not strictly the case (McDougall, 2003); however, with

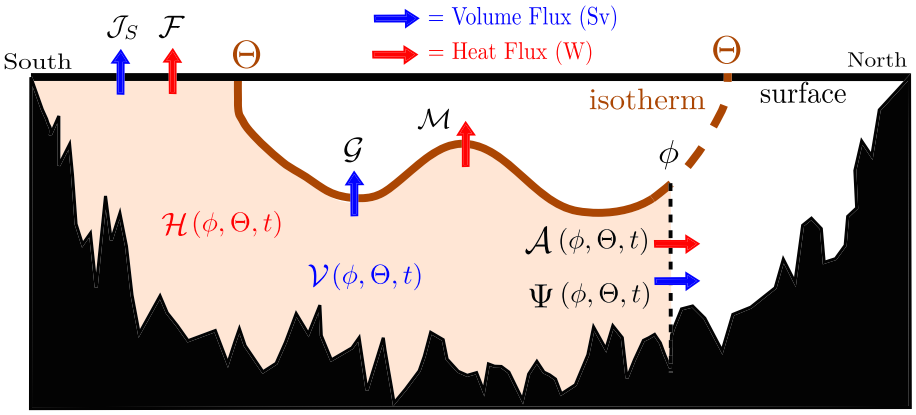

Figure 1. A schematic illustrating the heat and volume budgets of all water colder than some temperature Θ (marked by the brown isotherm) and south of some latitude ϕ (black dashed line). The volume $\mathcal{V}$ and heat content $\mathcal{H}$ of this region are functions of Θ, ϕ, and time t. All fluxes are also functions of Θ, ϕ, and t and are defined as positive if they are directed out of the volume $\mathcal{V}$. $\mathcal{F}$ denotes the surface heat fluxes (including the heat flux associated with the surface volume flux $\mathcal{J}_S$) and $\mathcal{M}$ denotes the heat fluxes across the Θ isotherm due to explicitly parameterized vertical mixing and numerical mixing. $\mathcal{G}$ denotes the volume flux across the Θ isotherm associated with water mass transformation. There are also volume $\Psi(\phi,\Theta,t)$ and heat $\mathcal{A}(\phi,\Theta,t)$ fluxes across the northern bounding latitude ϕ.

a variable $C_p\Theta$ all results would follow similarly), and $\frac{\partial\mathcal{V}}{\partial\Theta'}d\Theta'$ represents the volume within a given temperature interval $d\Theta'$ south of ϕ. Following HZE19, $\mathcal{H}$ can be integrated by parts and split into an external component,

$$\mathcal{H}_E(\phi,\Theta,t) = \rho_0 C_p \Theta \mathcal{V}, \tag{3}$$

and an internal component,

$$\mathcal{H}_I(\phi,\Theta,t) = -\rho_0 C_p \int_{-\infty}^{\Theta} \mathcal{V} d\Theta' = \rho_0 C_p \left(\overline{\Theta} - \Theta\right) \mathcal{V}, \tag{4}$$

where $\mathcal{H} = \mathcal{H}_I + \mathcal{H}_E$ and the last identity follows from $\mathcal{H} = \rho_0 C_p \overline{\Theta}\mathcal{V}$ where $\overline{\Theta} = \frac{1}{\mathcal{V}}\int_{-\infty}^{\Theta} \Theta'(\partial\mathcal{V}/\partial\Theta')d\Theta'$ is the volume averaged temperature. The internal component $\mathcal{H}_I$ is the heat content associated with the difference between the volume average temperature and the bounding temperature Θ (meaning that here $\mathcal{H}_I$ is always negative). Because of its dependence on a temperature difference, $\mathcal{H}_I$ is independent of the zero reference chosen for the temperature scale. In addition, the transport of $\mathcal{H}_I$ across the latitude ϕ, defined as $\mathcal{A}_I$ below, can be identified as the heat function of Ferrari and Ferreira (2011).

2.2. Transport of Internal Heat Content

The volume transport below the Θ isotherm defines a temperature stream function,

$$\Psi(\phi,\Theta,t) = \int\int_{\Theta'(x,\phi,z,t)<\Theta} v(x,\phi,z,t)dxdz, \tag{5}$$

where v is the meridional velocity (including any parameterized eddy-driven circulation) and the integral is performed following the time-varying temperature field Θ' at the latitude ϕ. The associated northward heat transport in Watts relative to 0 °C is

$$\mathcal{A}(\phi,\Theta,t) = \int_{-\infty}^{\Theta} \rho_0 C_p \Theta' \frac{\partial\Psi}{\partial\Theta'} d\Theta' + \mathcal{A}_D(\phi,\Theta,t), \tag{6}$$

where $\frac{\partial\Psi}{\partial\Theta'}d\Theta'$ represents the volume transport within a temperature interval $d\Theta'$ and $\mathcal{A}_D$ indicates any meridional heat transport that is not associated with the volume transport Ψ (e.g., the meridional component of parameterized diffusion).

The heat transport (equation (6)) can be integrated by parts, as for the heat content (equation (2)), and split into an external component,

$$\mathcal{A}_E(\phi,\Theta,t) = \rho_0 C_p \Theta \Psi, \tag{7}$$

and an internal component,

$$\mathcal{A}_I(\phi,\Theta,t) = -\rho_0 C_p \int_{-\infty}^{\Theta} \Psi d\Theta' + \mathcal{A}_D, \tag{8}$$

where $\mathcal{A} = \mathcal{A}_E + \mathcal{A}_I$. $\mathcal{A}_E$ would be the total heat transport if all of the fluid below Θ was isothermal. Thus, the internal component $\mathcal{A}_I$ captures the heat transport associated with variations in temperature within the layer. Once again, the internal heat content transport $\mathcal{A}_I$ is independent of the reference temperature used to define heat content and contributes to a simpler budget (see section 2.3). Note that the diffusive meridional heat transport $\mathcal{A}_D$ is part of $\mathcal{A}_I$ as it is not associated with a volume transport and depends only on temperature differences.

The internal heat content transport $\mathcal{A}_I$ in equation (8) is equivalent to the heat function of Ferrari and Ferreira (2011) (note that we use the opposite sign for Ψ). Differencing the heat function across a given circulation cell yields the meridional heat transport attributable to that cell. Evaluating the heat function at the maximum SST, $\Theta^{max}(\phi,t)$ (across all longitudes and seasons), captures the full depth circulation and thus yields the total meridional heat transport,

$$MHT(\phi,t) = \mathcal{A}_I(\phi,\Theta^{max},t). \tag{9}$$

The total external heat transport, $\mathcal{A}_E(\phi,\Theta^{max},t)$ is not included as it depends on the arbitrary reference temperature. Heat transport in the presence of a net volume transport is discussed in more detail in supplementary Text S3.

2.3. Diabatic Contributions to $\mathcal{A}_I$

The heat function $\mathcal{A}_I$ can also be related to the diabatic processes that alter the temperature of seawater parcels, leading to diathermal heat transports that contribute to the heat budget of the volume $\mathcal{V}$. The full heat content budget for this volume is (Figure 1),

$$\frac{\partial \mathcal{H}}{\partial t}(\phi,\Theta,t) = -\mathcal{F} - \mathcal{M} - \mathcal{A} - \rho_0 C_p \Theta \mathcal{G}, \tag{10}$$

where $\mathcal{F}$ denotes the heat flux out of the volume $\mathcal{V}$ associated with surface forcing, $\mathcal{A}$ is the heat transport across the latitude ϕ (equation (6)), $\mathcal{M}$ denotes the heat flux across the Θ isotherm associated with mixing processes and the last term is the heat flux associated with the volume flux across the Θ isotherm, $\mathcal{G}$. Following HZE19, equation (10) can be combined with the volume budget (Figure 1),

$$\frac{\partial \mathcal{V}}{\partial t}(\phi,\Theta,t) = -\mathcal{J}_S - \mathcal{G} - \Psi, \tag{11}$$

where $\mathcal{J}_S$ is the surface volume flux out of the volume $\mathcal{V}$, to yield a budget for the internal heat content (use equation (11) to substitute for $\mathcal{G}$ in equation (10)),

$$\frac{\partial \mathcal{H}_I}{\partial t}(\phi,\Theta,t) = -\mathcal{F}_I - \mathcal{M} - \mathcal{A}_I. \tag{12}$$

In equation (12), $\mathcal{F}_I = \mathcal{F} - \rho_0 C_p \Theta \mathcal{J}_S$ denotes the surface forcing corrected for the reference temperature dependent heat flux associated with surface volume fluxes (see HZE19 for more discussion). The internal heat content budget is not influenced by the volume flux across the Θ isotherm $\mathcal{G}$. This will be particularly important when analyzing the heat transport within the Atlantic or Indo-Pacific basins individually where $\mathcal{G}$ may be large, and it is not clear how to robustly assign a value of heat transport to it given its dependence on the reference temperature (equation (10)).

The budget equation (12) quantifies the relationship between the ocean's meridional heat transport, heat content tendency and the diabatic processes of surface forcing and mixing integrated over the volume $\mathcal{V}$. It can often be easier to interpret this budget by examining its local form that applies to a given infinitesimal region in the latitude-temperature plane (i.e., taking the Θ and ϕ derivative of equation (12)),

$$\frac{\partial}{\partial t}\left(\frac{\partial^2 \mathcal{H}_I}{\partial\Theta\partial\phi}\right) = -\frac{\partial}{\partial\Theta}\underbrace{\left(\frac{\partial \mathcal{F}_I}{\partial\phi} + \frac{\partial \mathcal{M}}{\partial\phi}\right)}_{\mathcal{J}_\Theta} - \frac{\partial}{\partial\phi}\underbrace{\left(\frac{\partial \mathcal{A}_I}{\partial\Theta}\right)}_{\mathcal{J}_\phi}, \tag{13}$$

where $\mathcal{J}_\Theta$ and $\mathcal{J}_\phi$ denote the local diathermal and meridional heat fluxes, respectively. Note that some processes, such as the along-isopycnal diffusion of temperature associated with eddy stirring, may have both a diathermal and a meridional (through $\mathcal{A}_D$ in equation (8)) component.

2.4. Global Ocean Sea Ice Model

We explore the heat transport and its dependence on diabatic processes using the *MOM025 Control* (1/4)° global ocean sea ice model used in HZE19. The model configuration is based on the ocean and sea ice components of the GFDL CM2.5 climate model (Delworth et al., 2012) and has 50 vertical levels. Repeating seasonally varying atmospheric forcing is taken from Version 2 of the Coordinated Ocean-ice Reference Experiment Normal Year Forcing (CORE-NYF, Large & Yeager, 2004). MOM025 Control does not include a parameterization for lateral or along-isopycnal temperature diffusion. Small-scale lateral temperature gradients are diffused by the numerical advection scheme, which is included in the mixing term $\mathcal{M}$ (see supporting information Text S2). The heat function and budget terms in equations (12)–(13) are diagnosed from the model heat budget terms binned online, at every time step, into 0.5 °C temperature bins. The details of these calculations, along with more information on the model configuration, are described in supporting information Text S1 and in HZE19.

3. The Temperature Structure of Heat Transport

The global stream function for volume transport in the temperature-latitude plane (Figure 2a) consists of an Antarctic Bottom Water cell south of 50°S, a North Atlantic Deep Water (NADW) cell between temperatures of 3 and 12 °C and northern and southern shallow subtropical cells at warmer temperatures. While all four cells carry a similar magnitude mass transport (reaching 20–30 Sv), the two deep cells cover a narrower temperature range and thus contribute less to the heat transport. This heat transport is quantified by the heat function $\mathcal{A}_I$ (Figure 2d). $\mathcal{A}_I$ contours describe the entrance of heat into the ocean at low latitudes, its movement poleward while descending toward colder temperatures, and the subsequent loss of heat back to the atmosphere at middle and high latitudes. In the meridional direction, this contour-following heat transport should be interpreted as the net effect of water moving in different directions at different temperatures. The net northward transport of internal heat content reaches 1.5 PW near 20°N, with a smaller southward maximum of 0.6 PW in the Southern Hemisphere (Figure 2d at warmest temperature, black line in Figure 3).

The heat function suggests that a large fraction of the meridional heat transport is achieved at warmer temperatures, where heat is supplied to the circulation (Figure 2d). The subtropical cells, which include components due to both vertical overturning and horizontal gyre circulation (we do not attempt to decompose the heat transport into horizontal and vertical components in this study; such a decomposition has been attempted elsewhere (e.g. Boccaletti et al., 2005)), play a major role as they span the large-temperature range of all waters warmer than ~12 °C (Ferrari & Ferreira, 2011; Klinger & Marotzke, 2000). While much of this heat transport occurs at temperatures that may be exposed to the atmosphere at some longitude and season (i.e., above the lower dotted black line in Figure 2 that indicates the minimum SST at each latitude), there is also a significant fraction that is associated with interior flow. In particular, at low-latitudes heat function contours have a downward, across-isotherm slope indicating the presence of interior diabatic processes. In contrast, the heat function contours at still colder temperatures associated with the NADW cell (below ~10 °C in Figure 2d) are more isothermal, indicating that diabatic processes are weaker.

Decomposing the global circulation into contributions from the Atlantic (Figures 2b and 2e) and Indo-Pacific (Figures 2c and 2f) basins individually reveals a story that is obscured in the global view. In a temperature coordinate the Indo-Pacific circulation consists largely of the two subtropical cells, with the Southern Hemisphere cell being stronger (due to stronger peak wind stresses in the Southern Hemisphere westerlies, Speich et al., 2007; Cessi, 2019) and spanning a larger temperature range. In contrast, the Atlantic is characterized by a clockwise circulation encompassing both the subtropical surface and NADW deep cells. These features have important implications for the heat transport in the two basins. The Atlantic transports heat northward at all latitudes (red line in Fig. [MHT], also see Ganachaud & Wunsch, 2003), with both deep and surface circulations contributing (Fig. [PsiAI]e Talley, 2003; Ferrari & Ferreira, 2011). In contrast the heat transport in the Indo-Pacific is more surface intensified while still overlapping in temperature with the Atlantic circulation in the Southern Hemisphere (Figure 2f, blue line in Figure 3). The southward heat transport out of the subtropical Indo-Pacific across 34°S exceeds the global southward heat transport there (compare black and blue lines in Figure 3), meaning that a significant fraction of this heat (~0.5 PW) must ultimately be a source for the northward heat transport in the Atlantic. The spatial structure of the surface heat flux implies that there must be a large transfer of heat from the Indo-Pacific to the Atlantic basin (also see Gordon, 1986), but, as discussed in the next section, this in turn requires that turbulent mixing diffuses heat into the temperature classes that experience net cooling in the surface North Atlantic. Note that the

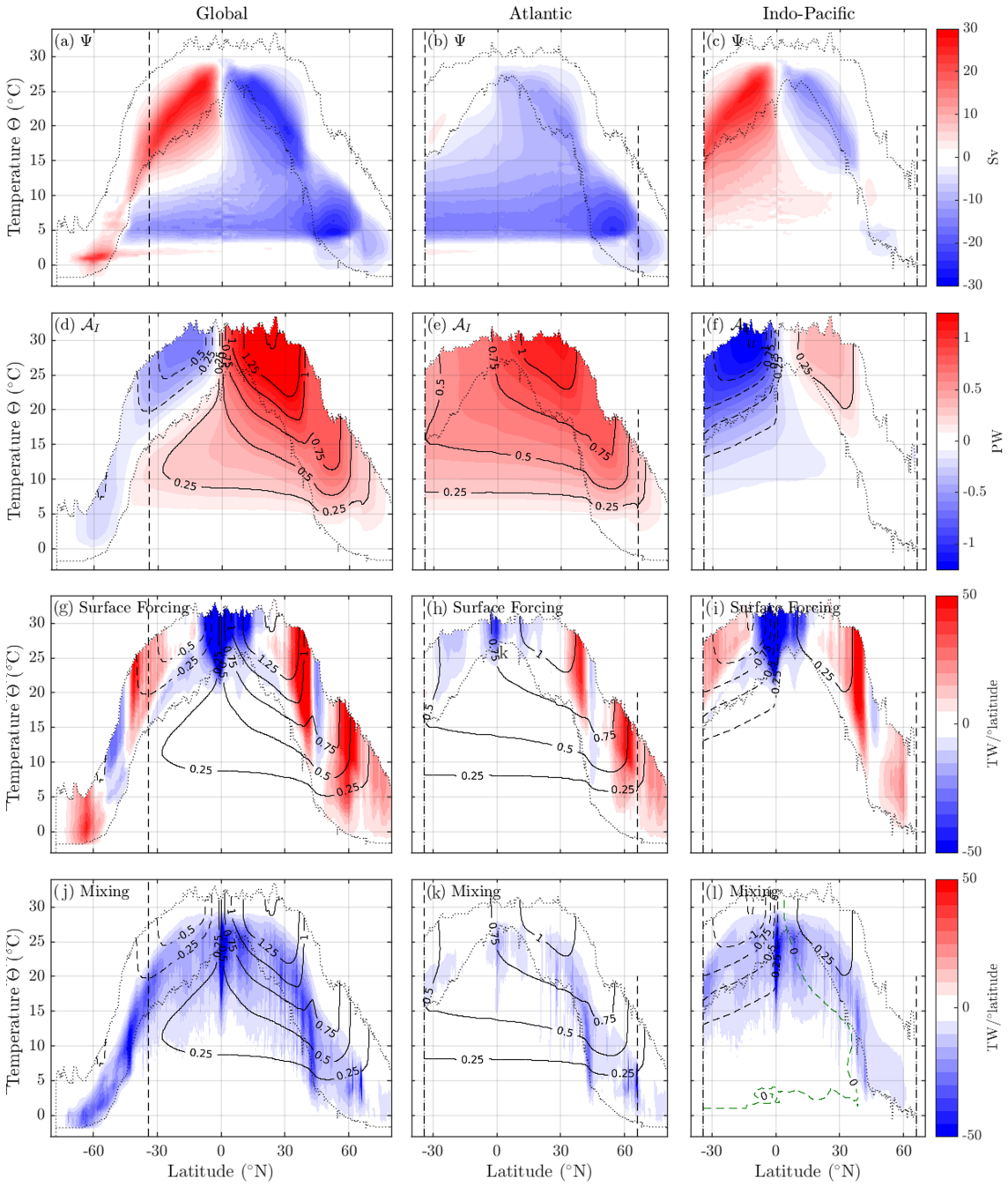

Figure 2. MOM025 Control (a–c) residual stream function Ψ in temperature coordinates (equation (5), Sv), (d–f) heat function $\mathcal{A}_I$ (equation (8), PW) and diathermal heat transports (TW/° latitude) due to (g–i) surface forcing ($\partial \mathcal{F}_I/\partial\phi$ in equation (13)) and (j–l) mixing ($\partial \mathcal{M}/\partial\phi$ in equation (13)) for (left column) all basins, (middle column) the Indo-Pacific, and (right column) the Atlantic. The thin dotted lines mark the minimum and maximum SST at each latitude at all zonal locations and seasons within the respective basin. The boundaries between the various basins are indicated by vertical dashed lines (including the Bering Strait at 66°N). The Arctic Ocean is included in the Atlantic. In panels (g)–(l) blue colors indicate fluxes toward colder temperature and the heat function $\mathcal{A}_I$ is shown in thin 0.25 PW contours for each basin, with the solid (dashed) contours indicating positive (negative) values.

net heat transports in the individual basins (Figure 3), as well as the temperature structure of these transports (Figure 2), compare well with the buoyancy transports discussed by Newsom & Thompson, 2018 (their Figures 2 and 4) outside the high-latitude Southern Ocean, showing that heat transport generally dominates the buoyancy transport in the upper ocean in these regions.

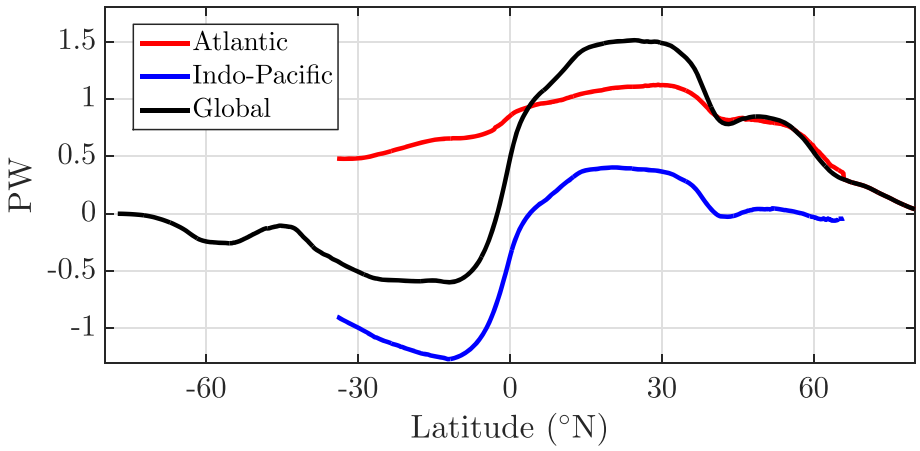

Figure 3. MOM025 Control global meridional heat transport (equation (9), PW, black line) and its Atlantic (red) and Indo-Pacific (blue) components.

4. Diabatic Contributions to Heat Transport

The net transport of heat from low to high latitudes captured by the heat function $\mathcal{A}_I$ could not occur without heat transport across temperature classes quantified by the diathermal heat flux $\mathcal{J}_\Theta$. $\mathcal{J}_\Theta$, the vertical vector component of the heat function contours in the temperature-latitude plane (equation (13)), contains contributions from surface forcing (Figures 2g–2i) and mixing (Figures 2j–2l). Surface heating in the equatorial regions between ±15° latitude acts as the main source of heat to the ocean circulation (Figure 2g). This heat uptake is dominated by the eastern equatorial Pacific cold tongue (1.09 PW of heat enters the region 10°S to 10°N, 165–70°W, not shown, see Figure 1a of HZE19), with a much smaller fraction entering the low-latitude Atlantic (0.36PW between 10°S-10°N across the Atlantic, compare Figs. [PsiAI]g-i, also see Newsom & Thompson, 2018). However, the Atlantic contributes much more substantially to surface heat loss. Much of this heat loss occurs poleward of 50°N (0.7 PW, compared to 0.11 PW north of 50°N in the Indo-Pacific), with heat loss also dominating over the Gulf Stream between 30°N and 45°N. Thus to maintain a steady state (the tendency in heat content is weak; Figure S1), the ocean circulation must arrange itself to connect the regions of heat gain and heat loss by exporting heat from the Indo-Pacific to the Atlantic. Note that the two-dimensional structure of the surface heat flux in the Southern Ocean indicates that heat loss in one zonal sector is not balanced by heat gain in another sector (not shown, see Figure 1a of HZE19), further supporting the need for interbasin heat exchange.

The patterns of surface heat uptake and surface heat loss imply not only a transport of heat from low latitudes to high latitudes and from the Indo-Pacific to the Atlantic but also from warm to cold temperatures (HZE19). The hot spot of heat loss in the high-latitude North Atlantic occurs at temperatures well below 18 °C, the maximum surface temperature there (Figure 2h), while low-latitude heating penetrates only to about 20 °C (Figure 2g). This highlights the essential role of mixing (Fig. [PsiAI]j-l, Speer & Tziperman, 1992). It is only through mixing that the regions of surface heat gain and loss can be connected, allowing heat to reach the cool isotherms that outcrop in the North Atlantic. Mixing accounts for much of the downward slope in the heat function contours within the cool branch of the subtropical cells. Without this mixing, the circulation cells would span a reduced temperature range and thus without a compensating increase in volume transport would transport less heat (Czaja & Marshall, 2006).

Much of the mixing, particularly at warmer temperatures, occurs in the Indo-Pacific basin (compare Figures 2j and 2l). This mixing contains contributions from a number of explicitly parameterized vertical mixing processes and numerical mixing, as discussed in more detail in supporting information Text S2 and HZE19. Mixing is less important in the Atlantic, where heat function contours follow more isothermal pathways (Figure 2k). The Southern Ocean appears to play a secondary role when considering heat transport alone (Figure 2j), as opposed to density-based water mass transformation. The diathermal heat flux associated with mixing is particularly strong at ±40° latitude. This is largely associated with numerical mixing (Figure S2d) and likely reflects the important role of mesoscale eddy stirring of along-isopycnal temperature gradients at these latitudes. If explicitly parameterized, this along-isopycnal eddy stirring would also

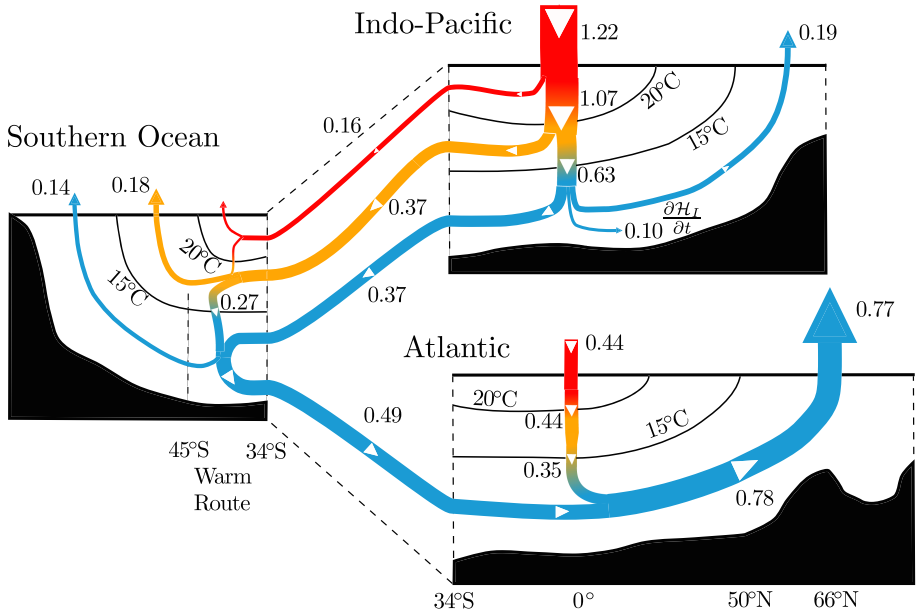

Figure 4. Summary of the internal heat content transports (in PW, with proportional line thickness) above, below, and across the 15 and 20 °C isotherm from MOM025 Control. Note that the maximum SST Θ^{max} replaces this upper isotherm bound (either 15 or 20 °C) in the case where it is colder, as described in supporting information Text S3. Arrows across the surface represent surface heat fluxes, arrows across the isotherms represent diffusive mixing, and horizontal arrows represent meridional internal heat content transports. Note that the isotherm outcrop positions (and the location of many of the heat fluxes) within each basin are somewhat arbitrary as water warmer and colder than 15 or 20 °C contacts the atmosphere over a range of latitudes. Heat transport pathways less than 0.1 PW are not shown (these account for the apparent mismatch between pathways).

contribute directly to the meridional heat flux there, in addition to the resolved meridional heat transport in $\mathcal{A}_I$.

5. North Atlantic Heat Transport Across 50°N

The heat transport pathways can be more precisely quantified by examining the total heat transport above and below carefully chosen isotherms. Here we choose the 15 and 20 °C isotherms (Figure 4), although a similar analysis could easily be applied to other isotherms. The 20 °C is chosen because it represents the coldest isotherm to which surface heating penetrates in the tropics (Figure 2g). The 15 °C is chosen because it captures the majority of the heat transport across 50°N into the North Atlantic and acts as an upper bound for the NADW overturning cell (Figure 2h). Approximately 40% (0.35 PW) of the 0.78 PW of heat transport across 50°N below 15 °C in the Atlantic is supplied by surface heat input in the tropical Atlantic followed by mixing across the 20 and 15 °C isotherms. The other 60% (0.49 PW) is supplied meridionally across 34°S at temperatures below 15 °C. All of this 0.49 PW is ultimately sourced from surface heat input at temperatures above 20 °C into the tropical Indo-Pacific (totaling 1.22 PW, Figure 4) via a pathway that relies on strong mixing across the 20 and 15 °C isotherms in the Indo-Pacific (1.07 and 0.63 PW, respectively). Mixing across the 15 °C isotherm within the "warm route" latitudes between 45°S and 34°S also contributes (0.27 PW).

The passage of heat from the warm tropical Indo-Pacific to the cold North Atlantic is the most obvious pathway in Figure 4, but other features are also evident. Heat transport into the North Pacific and its subsequent loss to the atmosphere is relatively small (0.19 PW below 15 °C). Model drift is evident in the buildup of heat below 15 °C in the Indo-Pacific (0.1 PW). Apart from a modest amount of net heat loss across all three temperature classes (and individually in both the Indo-Pacific and Atlantic sectors of the Southern Ocean, not shown), the high-latitude Southern Ocean appears to play a relatively passive role in the global heat transport (water-mass transformation here is dominated more by freshwater fluxes, e.g. Abernathey et al., 2016). Heat is transported northward throughout the Atlantic with weak net heat exchange with the Southern Ocean above 15 °C. There is also a small amount of heat transport through Bering Strait, associated with

the 1.03 Sv of volume transport from the Pacific into the Arctic. It is difficult to assign a precise value to this heat transport. In supporting information Text S3 we argue that its magnitude cannot exceed 0.08 PW.

6. Discussion

In this study we have quantified the contribution of different diabatic processes to heat transport in the temperature-latitude plane using a general framework based on the heat function of Ferrari and Ferreira (2011) and the internal heat content budget of HZE19. Applied to a (1/4)° global ocean sea ice model, the framework reveals the dominant global heat transport pathways as summarized in Figure 4. The ability to construct such a diagram relies on the use of internal heat content, which is independent of any arbitrary reference temperature.

The dominant heat transport pathway involves the movement of heat from the warm surface waters of the tropical Indo-Pacific (where the majority of warming via surface heat fluxes occurs, Figures 2g–2i, Figure 1a of HZE19) to the cold North Atlantic where heat is lost back to the atmosphere (Figure 4). This pathway depends critically on turbulent mixing which transfers heat out of the warm shallow tropical Indo-Pacific waters and supplies the upper branch of the AMOC with heat. 60% of the 0.78 PW of meridional heat transport across 50°N in the Atlantic below 15°C is supplied across 34°S at temperatures below 15 °C from the Indo-Pacific. As most heat enters the ocean at warmer temperatures, this implies that mixing in the Indo-Pacific (as well as some mixing in the warm route latitudes between 45 and 34 °S) plays a key role in converting NADW back to lighter intermediate and surface waters (e.g., Figure 2c) permitting the upper branch of the AMOC to transport heat northward.

The large exchange of heat between the Indo-Pacific and Atlantic is consistent with the results of Newsom and Thompson (2018) on buoyancy transport but differs somewhat from the conclusions of Forget and Ferreira (2019). The results of Forget and Ferreira (2019) suggest net heat fluxes into the Arctic-Atlantic basin of 0.29 PW (their Figure 1), compared to 0.4 PW in our study. This difference is linked to the surface heat flux pattern, and highlights the need to improve observational constraints on surface heat fluxes and to compare across a range of models. Analysis in this article is restricted to a single model with a specific set of parameterizations for diabatic processes. A similar MOM configuration with a refined resolution of (1/10)° shows a similar fractional contribution of Indo-Pacific heat uptake and mixing to Atlantic meridional heat transport but does not match observed meridional heat transport estimates as well as MOM025 Control (see supporting information Text S4). The framework we have introduced here provides a useful diagnostic tool that could be applied within future model intercomparisons to assess the sensitivity of ocean heat transport to different parameterizations.

This study highlights the key role of the tropical oceans, and in particular the tropical Indo-Pacific, for global ocean circulation and heat transport. There are a growing number of studies with this emphasis (e.g. Forget & Ferreira, 2019; Newsom & Thompson, 2018; Toggweiler et al., 2019). Here, we stress in particular the role of turbulent mixing in linking the heat transport associated with the shallow wind-driven Indo-Pacific circulation with the deeper-reaching Atlantic overturning circulation. The implications of this connection for the interannual and decadal variability of ocean heat transport remains an important area for future research, especially given the strong natural climate variability present in the tropical Indo-Pacific.

Acknowledgments
We thank A. Heerdegen, S. Griffies, and P. Spence for assistance with the modeling and diagnostics. This research was undertaken with the assistance of resources and services from the National Computational Infrastructure (NCI), which is supported by the Australian Government. This project was also supported by the Earth Science and Climate Change Hub of the Australian Government's National Environmental Science Program (NESP) and the Centre for Southern Hemisphere Oceans Research (CSHOR), a joint research center between QNLM, CSIRO, UNSW, and UTAS. The data required to reproduce the results in this article are published online at Research Data Australia (Holmes et al., 2019, https://doi.org/10.26190/5dc23d4b7e739).

References

Abernathey, R. P., Cerovecki, I., Holland, P. R., Newsom, E., Mazloff, M., & Talley, L. D. (2016). Water-mass transformation by sea ice in the upper branch of the Southern Ocean overturning. *Nature Geoscience*, *9*(8), 596–601. https://doi.org/10.1038/ngeo2749

Boccaletti, G., Ferrari, R., Adcroft, A., Ferreira, D., & Marshall, J. (2005). The vertical structure of ocean heat transport. *Geophysical Research Letters*, *32*, L10603. https://doi.org/10.1029/2005GL022474

Cessi, P. (2019). The global overturning circulation. *Annual Review of Marine Science*, *11*(1), 249–270. https://doi.org/10.1146/annurev-marine-010318-095241

Czaja, A., & Marshall, J. (2006). The partitioning of poleward heat transport between the atmosphere and ocean. *Journal of the Atmospheric Sciences*, *63*(5), 1498–1511. https://doi.org/10.1175/JAS3695.1

Delworth, T. L., Rosati, A., Anderson, W., Adcroft, A. J., Balaji, V., Benson, R., et al. (2012). Simulated climate and climate change in the GFDL CM2.5 high-resolution coupled climate model. *Journal of Climate*, *25*(8), 2755–2781. https://doi.org/10.1175/JCLI-D-11-00316.1

Ferrari, R., & Ferreira, D. (2011). What processes drive the ocean heat transport? *Ocean Modelling*, *38*(3-4), 171–186. https://doi.org/10.1016/j.ocemod.2011.02.013

Ferrari, R., Nadeau, L.-P., Marshall, D. P., Allison, L. C., & Johnson, H. L. (2017). A model of the ocean overturning circulation with two closed basins and a re-entrant channel. *Journal of Physical Oceanography*, *47*, 2887–2906. https://doi.org/10.1175/JP0-D-16-0223.1

Ferrari, R., & Wunsch, C. (2009). Ocean circulation kinetic energy: Reservoirs, sources, and sinks. *Annual Review of Fluid Mechanics*, *41*, 253–282. https://doi.org/10.1146/annurev.fluid.40.111406.102139

Forget, G., & Ferreira, D. (2019, April). Global ocean heat transport dominated by heat export from the tropical Pacific. *Nature Geoscience.*. https://doi.org/10.1038/s41561-019-0333-7

Ganachaud, A., & Wunsch, C. (2003). Large-scale ocean heat and freshwater transports during the World Ocean Circulation Experiment. *Journal of Climate*, *16*(4), 696705. https://doi.org/10.1175/1520-0442(2003)016(0696:LS0HAF)2.0.C0;2

Gnanadesikan, A. (1999). A simple predictive model for the structure of the oceanic pycnocline. *Science*, *283*(5410), 2077–2079. https://doi.org/10.1126/science.283.5410.2077

Gordon, A. L. (1986). Interocean exchange of thermocline water. *Journal of Geophysical Research*, *91*(C4), 5037–5046. https://doi.org/10.1029/JC091iC04p05037

Gordon, A. L., Weiss, R. F., Smethie, W. M. Jr., & Warner, M. J. (1992). Thermocline and intermediate water communication between the South Atlantic and Indian oceans. *Journal of Geophysical Research*, *97*(C5), 7223–7240. https://doi.org/10.1029/92JC00485

Greatbatch, R. J., & Zhai, X. (2007). The generalized heat function. *Geophysical Research Letters*, *34*, L21601. https://doi.org/10.1029/2007GL031427

Gregory, J. M. (2000). Vertical heat transports in the ocean and their effect on time-dependent climate change. *Climate Dynamics*, *16*(7), 501–515. https://doi.org/10.1007/s003820000059

Hieronymus, M., Nilsson, J., & Nycander, J. (2014). Water mass transformation in salinity-temperature space. *Journal of Physical Oceanography*, *44*(9), 2547–2568. https://doi.org/10.1175/JP0-D-13-0257.1

Hochet, A., & Tailleux, R. (2019). Comments on "Diathermal heat transport in a global ocean model". *Journal of Physical Oceanography*, *49*(8), 2189–2193. https://doi.org/10.1175/JPO-D-19-0055.1

Holmes, R. M., Zika, J. D., & England, M. H. (2019a). Diathermal heat transport in a global ocean model. *Journal of Physical Oceanography*, *49*(1), 141–161. https://doi.org/10.1175/JP0-D-18-0098.1

Holmes, R. M., Zika, J. D., & England, M. H. (2019b). Reply to'Comments on "Diathermal heat transport in a global ocean model". *Journal of Physical Oceanography*, *49*(8), 2195–2197. https://doi.org/10.1175/JP0-D-19-0139.1

Holmes, R. M., Zika, J. D., Ferrari, R., Thompson, A., Newsom, E., & England, M. H. (2019). Atlantic ocean heat transport enabled by Indo-Pacific heat uptake and mixing. UNSW dataset, Research Data Australia https://doi.org/10.26190/5dc23d4b7e739

Klinger, B. A., & Marotzke, J. (2000). Meridional heat transport by the subtropical cell. *Journal of Physical Oceanography*, *30*(4), 696–705. https://doi.org/10.1175/1520-0485(2000)030(0696:MHTBTS)2.0.C0;2

Large, W. G., & Yeager, S. (2004). Diurnal to decadal global forcing for ocean and sea-ice models: the data sets and flux climatologies. National Center for Atmospheric Research.

Large, W. G., & Yeager, S. G. (2009). The global climatology of an interannually varying air-sea flux data set. *Climate Dynamics*, *33*(2), 341–364. https://doi.org/10.1007/s00382-008-0441-3

Lee, S.-K., Lumpkin, R., Baringer, M. O., Meinen, C. S., Goes, M., Dong, S., et al. (2018). Global meridional overturning circulation inferred from a data-constrained ocean & sea-ice model. *Geophysical Research Letters*, *46*, 1521–1530. https://doi.org/10.1029/2018GL080940

Marshall, J., & Speer, K. (2012). Closure of the meridional overturning circulation through Southern Ocean upwelling. *Nature Geoscience*, *5*(3), 171–180. https://doi.org/10.1038/ngeo1391

McDougall, T. J. (2003). Potential enthalpy: A conservative oceanic variable for evaluating heat content and heat fluxes. *Journal of Physical Oceanography*, *33*(5), 945–963. https://doi.org/10.1175/1520-0485(2003)033(0945:PEACOV)2.0.CO;2

Newsom, E. R., & Thompson, A. F. (2018). Reassessing the role of the Indo-Pacific in the ocean's global overturning circulation. *Geophysical Research Letters*, *45*, 12,422–12,431. https://doi.org/10.1029/2018GL080350

Niiler, P., & Stevenson, J. (1982). The heat budget of tropical ocean warm-water pools. *Journal of Marine Research*, *40*, 465–480.

Rintoul, S. R. (1991). South atlantic interbasin exchange. *J. Geophys. Res.*, *96*(C2), 2675–2692. https://doi.org/10.1029/90JC02422

Saenko, O. A., Yang, D., & Gregory, J. M. (2018). Impact of mesoscale eddy transfer on heat uptake in an eddy-parameterizing ocean model. *Journal of Climate*, *31*(20), 8589–8606. https://doi.org/10.1175/JCLI-D-18-0186.1

Speer, K., & Tziperman, E. (1992). Rates of water mass formation in the north Atlantic ocean. *Journal of Physical Oceanography*, *22*(1), 93–104. https://doi.org/10.1175/1520-0485(1992)022(0093:ROWMFI)2.0.CO;2

Speich, S., Blanke, B., & Cai, W. (2007). Atlantic meridional overturning circulation and the Southern Hemisphere supergyre. *Geophysical Research Letters*, *34*, L23614. https://doi.org/10.1029/2007GL031583

Talley, L. (2013). Closure of the global overturning circulation through the Indian, Pacific, and Southern Oceans: Schematics and transports. *Oceanography*, *26*, 80–97.

Talley, L. D. (2003). Shallow, intermediate, and deep overturning components of the global heat budget. *Journal of Physical Oceanography*, *33*(3), 530–560. https://doi.org/10.1175/1520-0485(2003)033(0530:SIAD0C)2.0.C0;2

Thompson, A. F., Stewart, A. L., & Bischoff, T. (2016). A multi-basin residual-mean model for the global overturning circulation. *Journal of Physical Oceanography*, *46*(9), 2583–2604. https://doi.org/10.1175/JPO-D-15-0204.1

Toggweiler, J. R., Druffel, E. R. M., Key, R. M., & Galbraith, E. D. (2019). Upwelling in the ocean basins north of the ACC Part 2: How cool subantarctic water reaches the surface in the tropics. *Journal of Geophysical Research: Oceans*, *124*, 2609–2625. https://doi.org/10.1029/2018JC014795

Trenberth, K. E., & Caron, J. M. (2001). Estimates of meridional atmosphere and ocean heat transports. *Journal of Climate*, *14*(16), 3433–3443. https://doi.org/10.1175/1520-0442(2001)014(3433:E0MAA0)2.0.C0;2

Trenberth, K. E., Zhang, Y., Fasullo, J. T., & Cheng, L. (2019). 0bservation-based estimates of global and basin ocean meridional heat transport time series. *Journal of Climate*, *32*(14), 4567–4583. https://doi.org/10.1175/JCLI-D-18-0872.1

Valdivieso, M., Haines, K., Balmaseda, M., Chang, Y.-S., Drevillon, M., Ferry, N., et al. (2017). An assessment of air-sea heat fluxes from ocean and coupled reanalyses. *Climate Dynamics*, *49*(3), 983–1008. https://doi.org/10.1007/s00382-015-2843-3

Vallis, G. K., & Farneti, R. (2009). Meridional energy transport in the coupled atmosphere-ocean system: Scaling and numerical experiments. *Quarterly Journal of the Royal Meteorological Society*, *135*(644), 1643–1660. https://doi.org/10.1002/qj.498

Yang, H., Li, Q., Wang, K., Sun, Y., & Sun, D. (2015). Decomposing the meridional heat transport in the climate system. *Climate Dynamics*, *44*(9), 2751–2768. https://doi.org/10.1007/s00382-014-2380-5

Zika, J. D., Laliberte, F., Mudryk, L. R., Sijp, W. P., & Nurser, A. J. G. (2015). Changes in ocean vertical heat transport with global warming. *Geophysical Research Letters*, *42*, 4940–4948. https://doi.org/10.1002/2015GL064156

Zika, J. D., Sijp, W. P., & England, M. H. (2013). Vertical heat transport by ocean circulation and the role of mechanical and haline forcing. *Journal of Physical Oceanography*, *43*(10), 2095–2112. https://doi.org/10.1175/JP0-D-12-0179.1

References From the Supporting Information

Colella, P., & Woodward, P. R. (1984). The piecewise parabolic method (ppm) for gas-dynamical simulations. *J. Comput. Phys.*, *54*(1), 174–201. https://doi.org/10.1016/0021-9991(84)90143-8

Fox-Kemper, B., Ferrari, R., & Hallberg, R. (2008). Parameterization of mixed layer eddies. Part I: Theory and diagnosis. *J. Phys. Oceanogr.*, *38*(6), 11451165. https://doi.org/10.1175/2007JP03792.1

Griffies, S. M. (1998). The Gent-McWilliams skew flux. *Journal of Physical Oceanography*, *28*(5), 831–841. https://doi.org/10.1175/1520-0485(1998)028(0831:TGMSF)2.0.C0;2

Hieronymus, M., Nycander, J., Nilsson, J., Doos, K., & Hallberg, R. (2019). 0ceanic overturning and heat transport: The role of background diffusivity. *J. Climate*, *32*(3), 701–716. https://doi.org/10.1175/JCLI-D-18-0438.1

Large, W. G., McWilliams, J. C., & Doney, S. C. (1994). Oceanic vertical mixing: A review and a model with a nonlocal boundary layer parameterization. *Rev. Geophys.*, *32*(4), 363–403. https://doi.org/10.1029/94RG01872

Simmons, H. L., Jayne, S. R., Laurent, L. C. S., & Weaver, A. J. (2004). Tidally driven mixing in a numerical model of the ocean general circulation. *Ocean Model.*, *6*(3), 245–263. https://doi.org/10.1016/S1463-5003(03)00011-8

Suresh, A., & Huynh, H. (1997). Accurate monotonicity-preserving schemes with Runge-Kutta time stepping. *J. Comput. Phys.*, *136*(1), 83–99. https://doi.org/10.1006/jcph.1997.5745

Vranes, K., Gordon, A. L., & Ffield, A. (2002). The heat transport of the Indonesian Throughflow and implications for the Indian 0cean heat budget. *Deep Sea Research Part II: Topical Studies in Oceanography*, *49*(7), 1391–1410. https://doi.org/10.1016/S0967-0645(01)00150-3

Woodgate, R. A. (2018). Increases in the Pacific inflow to the Arctic from 1990 to 2015, and insights into seasonal trends and driving mechanisms from year- round Bering Strait mooring data. *Progress in Oceanography*, *160*, 124–154. https://doi.org/10.1016/j.pocean.2017.12.007

Supporting Information for "Atlantic ocean heat transport enabled by Indo-Pacific heat uptake and mixing"

Ryan M. Holmes[1,2], Jan D. Zika[2], Raffaele Ferrari[3], Andrew F. Thompson[4],

Emily R. Newsom[5], and Matthew H. England[1]

[1]Climate Change Research Centre and the ARC Centre of Excellence for Climate Extremes, University of New South Wales, Sydney, NSW, Australia

[2]School of Mathematics and Statistics, University of New South Wales, Sydney, NSW, Australia

[3]Department of Earth, Atmosphere and Planetary Sciences, Massachusetts Institute of Technology, Cambridge, Massachusetts, U.S.A.

[4]Environmental Science and Engineering, California Institute of Technology, Pasadena, California, U.S.A.

[5]Department of Physics, University of Oxford, Oxford, United Kingdom

Contents of this file

Introduction

Corresponding author: R. M. Holmes, Climate Change Research Centre, University of New South Wales, Sydney, NSW, Australia (ryan.holmes@unsw.edu.au)

The supporting information contains a number of supplementary figures referred to in the main article as well as brief discussions of the model configuration and numerical details of the diagnostic calculations (text S1), the contribution of various parameterized mixing processes to the total mixing (text S2), a discussion of heat transport in the presence of a net meridional volume transport through Bering Strait (text S3) and a comparison of the model meridional heat transport to observational products (text S4).

Text S1: Model details and the numerical diagnostic calculations

The model configuration used is the MOM025 Control simulation of HZE19. Vertical mixing, captured within the term $\mathcal{M}$ in Eq. 10, is parameterized using the K-profile parameterization (Large, McWilliams, & Doney, 1994), a bottom-enhanced internal tide mixing scheme (Simmons, Jayne, Laurent, & Weaver, 2004) and a background vertical diffusivity. The MOM025 Control background diffusivity κ_B is latitude dependent being $10^{-5}\mathrm{m}^2\mathrm{s}^{-1}$ poleward of 15° latitude and reducing linearly to $10^{-6}\mathrm{m}^2\mathrm{s}^{-1}$ within 5° of the Equator. MOM025 Control was initialized from the end of a similar 500 year simulation with no background diffusivity (the $\kappa_B = 0$ case considered by HZE19) and then run for an additional 111 years to equilibrate to the change in κ_B. Analysis comes from the last 10 years.

We use the same methods to calculate the diathermal fluxes as in HZE19. However, here the latitudinally-resolved heat budget also includes lateral heat transports, which were zero by definition in the globally-integrated budget of HZE19. The stream function Ψ is obtained by accumulating the volume transport within 0.5°C temperature bins online at each grid point, as for the other diagnostics. We tested several methods of calculating

the internal heat content transport $\mathcal{A}_I$. The best method was found to be subtracting the external heat transport component $\mathcal{A}_E$ [Eq. 7] from the total meridional heat transport $\mathcal{A}(\phi, \Theta, t)$ calculated by accumulating the meridional heat flux relative to 0°C within each temperature bin online. Other methods, such as calculating $\mathcal{A}_I$ by directly integrating the stream function [via Eq. 8] yielded similar results, with a higher level of noise.

MOM025 Control does not include a mesoscale eddy parameterization or explicit isopycnal or lateral diffusion. The suppression of large lateral tracer gradients is thus achieved by the multi-dimensional piece-wise parabolic tracer advection scheme (Colella and Woodward (1984), with a monotonicity-preserving flux limiter following Suresh and Huynh (1997)). As in HZE19 the across-isotherm diffusive heat flux associated with the numerical advection scheme (referred to as numerical mixing) is calculated by residual. Here it is included in the mixing term $\mathcal{M}$ (see supplementary text S2).

The model configuration also includes a parameterization for submesoscale restratification (Fox-Kemper, Ferrari, & Hallberg, 2008). This parameterization is implemented through skew-diffusion (Griffies, 1998), and therefore is not associated with any explicit volume circulation (i.e. it does not alter Ψ). Hence, its influence on the internal heat content budget is through its meridional heat flux included in $\mathcal{A}_D$ as part of $\mathcal{A}_I$ in Eq. 8. While skew-diffusion should not result in any across-isotherm fluxes of heat, its numerical implementation may induce some such fluxes, which are included in the numerical mixing flux across isotherms.

Text S2: The processes contributing to mixing

The diathermal heat transport arising from mixing contains contributions from a number of explicitly-parameterized vertical mixing processes (Fig. S2a-c,e,f) and numerical mixing (Fig. S2d). The strongest vertical mixing fluxes are focused very close to the Equator between 15°C and 28°C and are associated with shear instability (Fig. S2c) in the eastern equatorial Pacific cold tongue (e.g. see Fig. 4c of HZE19). Background mixing is significant across most of the temperature-latitude plane, in particular in the interior subtropical regions, driving most of the diathermal heat flux in those regions responsible for the downward slope in the heat function (e.g. compare Fig. 2d and Fig. S2b between 15°C and 20°C in the latitude range 10°-30° in both hemispheres). Background mixing is also strong around the surface outcrop regions at all latitudes. The sensitivity of the diathermal heat transport to the background diffusivity is examined in HZE19 (also see Hieronymus, Nycander, Nilsson, Döös, & Hallberg, 2019). Boundary layer mixing is relatively uniformly distributed with latitude and focused around the surface outcrops (Fig. S2e), although there is also a peak around the Equator associated with the eastern equatorial Pacific cold tongue (e.g. see Fig. 4d of HZE19). Mixing associated with the bottom-intensified tidal mixing scheme of Simmons et al. (2004) is relatively uniform with temperature and focused in the tropics and mid-latitudes, although there are also peaks in the high northern latitudes (Fig. S2f).

Numerical mixing (see text S1) also makes a significant contribution to the diathermal heat transport (Fig. S2d). As discussed in more detail in HZE19, the large contribution of numerical mixing arises because sources of explicit mixing have been minimized in this model configuration (e.g. the lack of any explicit lateral mixing) in order to minimize

the overall levels of mixing. Numerical mixing drives down-gradient heat fluxes that are peaked in the equatorial regions at temperatures above ~ 15°C and along the mid-latitude outcrop regions. The peak near the equator is likely associated with the strong vertical temperature gradients and vertical velocity variability in that region. The numerical mixing at higher latitudes near the surface outcrops, which in many cases is stronger than the explicit vertical mixing, may be associated with along-isopycnal eddy stirring and the subsequent dissipation of along-isopycnal temperature gradients that is not explicitly parameterized. The structure and causes of numerical mixing will be examined in more detail in a forthcoming article.

Text S3: Heat transport in the presence of a net meridional volume transport through Bering Strait

The presence of a net lateral volume transport (through a passage such as the Bering Strait) introduces some ambiguity into the meaning and value of the associated heat transport. In MOM025 Control there is a mean transport of $\Psi_{BS}(\Theta^{max}) = +1.03$Sv through Bering Strait, where the maximum SST is $\Theta^{max} = 10.5$°C. The associated total internal heat content transport below Θ^{max} is southward (due to the negative sign in Eq. 8) with value -0.04PW, in the opposite direction to the volume transport. This southward heat transport arises because, as defined in Eq. 8, the internal heat content transport evaluated at some value of Θ greater than or equal to Θ^{max} inherently assumes that water returns back through the Bering Strait, closing the circulation, at temperature Θ. This also implies that the magnitude of the internal heat content transport continues to increase when evaluated at temperatures Θ greater than Θ^{max} (i.e. $\mathcal{J}_\phi = \frac{\partial \mathcal{A}_I}{\partial \Theta}$ is non-

zero even at temperatures greater than Θ^{max}). As the volume flux through Bering Strait is largely closed by passage through the Indo-Pacific and Atlantic basins via the Southern Ocean (while also being modified by surface volume fluxes), this heat flux ambiguity also affects the heat budgets of these basins.

For the purposes of the schematic in Fig. 4 the heat budget of each layer is constructed between the cooler isotherm (e.g. 15°C for the 15° to 20°C layer) and the colder of either the warm isotherm or the maximum SST Θ^{max} at each latitude (upper thin dotted line in Fig. 2). The temperature of the upper boundary of the layer thus varies with latitude, meaning that to close the heat budget of the layer the meridional component of the heat transport, $\frac{\partial \mathcal{A}_I}{\partial \Theta}(\phi, \Theta^{max}, t)$, exiting this upper boundary must be taken into account. For the purposes of Fig. 4, this heat transport is included as part of the surface forcing term. The changes to Fig. 4 resulting from this procedure (compared to using the upper isotherm Θ even when it is warmer than Θ^{max}) are minimal and are restricted to the transport through Bering Strait (as discussed next) and some small changes to the high-latitude surface heat fluxes and the southward transport above 20°C across 34°S out of the Indo-Pacific.

A bound for the effective magnitude of the heat transport through the Bering Strait, corresponding to a bound for the ambiguity on the Indo-Pacific and Atlantic heat budgets, can be constructed by matching the Bering Strait volume and heat transport with estimates of the return transport via the Southern Ocean (e.g. see Vranes, Gordon, & Ffield, 2002, who discuss the Indonesian Throughflow heat transport). The net heat transport

associated with the Bering Strait volume transport Ψ_{BS} is,

$$MHT_{BS} = \rho_0 C_p \left(\overline{\Theta}_{BS} - \overline{\Theta}_{SO}\right) \Psi_{BS}(\Theta^{max}), \tag{1}$$

where $\overline{\Theta}_{BS}$ and $\overline{\Theta}_{SO}$ are transport weighted temperatures through the Bering Strait and the return pathway via the Southern Ocean. Using the MOM025 Control Bering Strait mass transport ($\Psi_{BS} = +1.03$Sv) and heat transport relative to 0°C ($\mathcal{A}_{BS} = +0.003$PW), we find that $\overline{\Theta}_{BS} = \mathcal{A}_{BS}/\left(\rho_0 C_p \Psi_{BS}\right) = 0.76$°C. However, $\overline{\Theta}_{SO}$ is uncertain, as it depends on which portion of the heat transport via the return pathway through the Southern Ocean is matched to Ψ. Considering values of $\overline{\Theta}_{SO}$ in the large range −2°C to 20°C yields a range for MHT_{BS} of between −0.08 and +0.01PW. Observations suggest that this heat transport does not exceed 0.02PW, using a reference temperature of −1.9°C (Woodgate, 2018). These values are less than the minimum transport of 0.1PW shown in Fig. 4, and thus the ambiguity is relatively small. However, for passages where the net volume transport is much larger the associated ambiguity is also much larger. For this reason we do not examine in detail the heat transports through Drake Passage or the Indonesian Throughflow.

Text S4: Heat transport comparison with observational estimates and a fine resolution model

The MOM025 Control meridional heat transport (solid lines in Fig. S3) compares favorably with both direct and indirect observational estimates (dashed lines and markers with error bars in Fig. S3, Ganachaud & Wunsch, 2003; Trenberth, Zhang, Fasullo, & Cheng, 2019). The Atlantic heat transport in particular is well represented (red lines in Fig. S3). The southward heat transport in the Southern Hemisphere Indo-Pacific is weaker than

observations suggest. This appears to be a common problem with many global ocean models, and it remains unclear whether this problem is linked to model biases or observational errors (e.g. Griffies et al., 2009; Trenberth & Caron, 2001; Valdivieso et al., 2017). A similar MOM-SIS configuration with a finer horizontal resolution of 1/10° (MOM01, which also has 75 vertical levels instead of 50, and no background vertical diffusivity) has similar heat transport in the Indo-Pacific but significantly weaker transport in the Atlantic (thin solid lines in Fig. S3), which is linked to a weaker NADW circulation (not shown). Hence we have chosen to focus on MOM025 Control in this study. Nevertheless, a similar analysis to that performed in the main article applied to MOM01 shows that the contribution of Indo-Pacific heat uptake and mixing to Atlantic meridional heat transport remains similar. 52% (0.28PW) of the 0.54PW of northward heat transport across 50°N in the Atlantic in MOM01 is supplied across 34°S ultimately from temperatures above 20°C in the Indo-Pacific, while 0.19PW is supplied through mixing across the 15°C isotherm in the Atlantic. Thus our qualitative conclusions are robust to the differences between MOM01 and MOM025 Control.

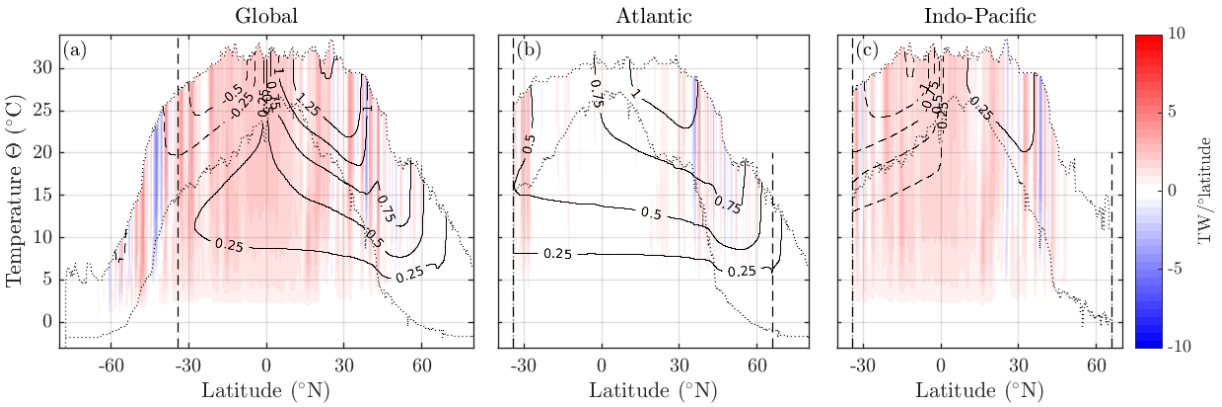

Figure S1. MOM025 Control (a) global, (b) Atlantic and (c) Indo-Pacific internal heat content tendency $[\partial/\partial t\,(\partial\mathcal{H}_I/\partial\phi)$, TW/° latitude]. At each temperature the color corresponds to the net flux of heat into all fluid colder than that temperature within each latitude band. The heat function $\mathcal{A}_I$ is shown in thin black 0.25PW contours for each basin, with the solid (dashed) contours indicating positive (negative) values. The thin dotted lines mark the minimum and maximum SST at each latitude at all zonal locations and seasons within each basin.

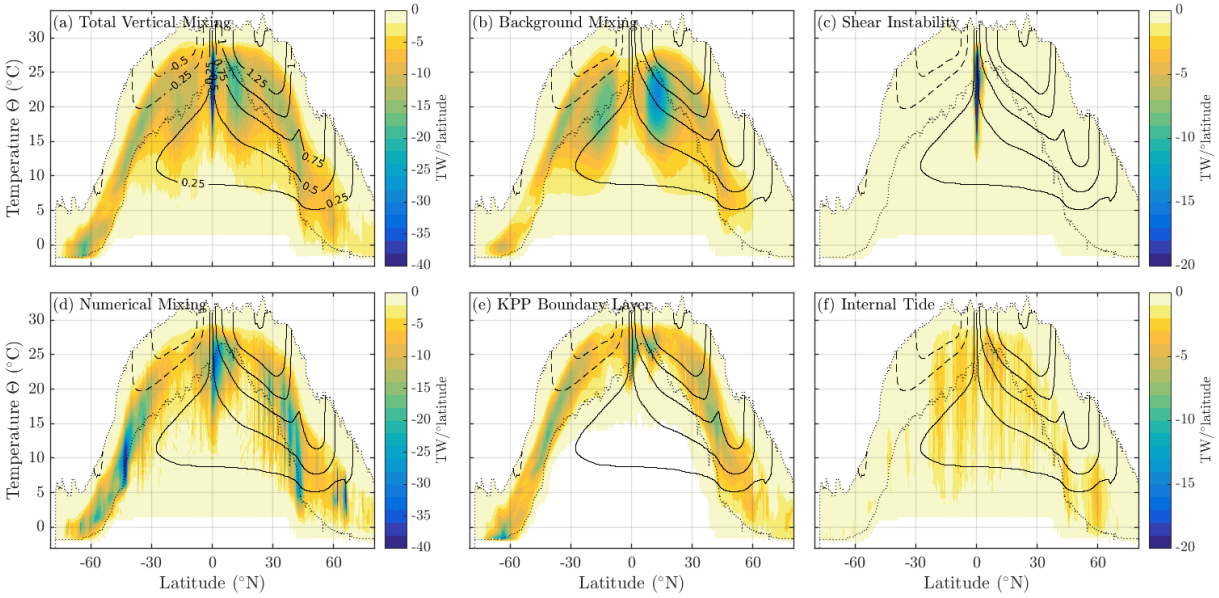

Figure S2. The MOM025 Control global diathermal heat transport due to mixing ($\partial\mathcal{M}/\partial\phi$ in Eq. (13), Fig. 3d) decomposed into its components due to (a) explicitly parameterized total vertical mixing and (d) numerical mixing. The explicitly parameterized vertical mixing (panel a) includes components due to (b) background mixing, (c) interior shear instability, (e) boundary layer mixing and (f) internal tide mixing and several other small processes (e.g. double-diffusion, not shown). The heat function is shown in black 0.25PW contours. The thin dotted lines mark the zonal minimum and maximum SST at each latitude at all zonal locations and seasons.

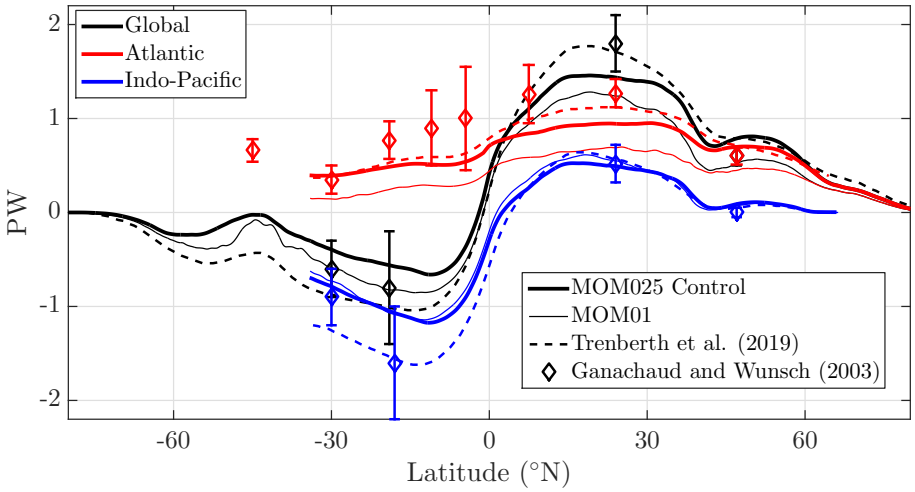

Figure S3. Total meridional heat transport in MOM025 Control (thick solid lines), MOM01 (thin solid lines) and from observational estimates from a World Ocean Circulation Experiment inversion (Ganachaud & Wunsch, 2003, markers with error bars) and from reanalysis data (Trenberth et al., 2019, dashed lines). Note that here, as opposed to in Fig. 2 of the main article, all curves represent the total heat transport relative to a reference temperature of 0°C.